Received: 21 May 2020 | Accepted: 7 July 2020

DOI: 10.1111/gcb.15279

PRIMARY RESEARCH ARTICLE

Global Change Biology WILEY

Climate regime shift and forest loss amplify fire in Amazonian forests

Xiyan Xu[1] | Gensuo Jia[1] | Xiaoyan Zhang[2] | William J. Riley[3] | Ying Xue[4]

[1]Key Laboratory of Regional Climate-Environment for Temperate East Asia, Institute of Atmospheric Physics, Chinese Academy of Sciences, Beijing, China

[2]School of Atmospheric Science, Nanjing University of Information Science and Technology, Nanjing, China

[3]Climate and Ecosystem Sciences Division, Lawrence Berkeley National Laboratory, Berkeley, CA, USA

[4]School of Applied Meteorology, Nanjing University of Information Science and Technology, Nanjing, China

Correspondence
Xiyan Xu and Gensuo Jia, Key Laboratory of Regional Climate-Environment for Temperate East Asia, Institute of Atmospheric Physics, Chinese Academy of Sciences, Beijing 100029, China.
Email: xiyan.xu@tea.ac.cn (X. X.); jiong@tea.ac.cn (G. J.)

Funding information
Natural Science Foundation of China, Grant/Award Number: 41875107; National Key R&D Program of China, Grant/Award Number: 2018YFA0606002; Chinese Academy of Sciences, Grant/Award Number: XDA19030401; U.S. Department of Energy, Grant/Award Number: DE-AC02-05CH11231

Abstract

Frequent Amazonian fires over the last decade have raised the alarm about the fate of the Earth's most biodiverse forest. The increased fire frequency has been attributed to altered hydrological cycles. However, observations over the past few decades have demonstrated hydrological changes that may have opposing impacts on fire, including higher basin-wide precipitation and increased drought frequency and severity. Here, we use multiple satellite observations and climate reanalysis datasets to demonstrate compelling evidence of increased fire susceptibility in response to climate regime shifts across Amazonia. We show that accumulated forest loss since 2000 warmed and dried the lower atmosphere, which reduced moisture recycling and resulted in increased drought extent and severity, and subsequent fire. Extremely dry and wet events accompanied with hot days have been more frequent in Amazonia due to climate shift and forest loss. Simultaneously, intensified water vapor transport from the tropical Pacific and Atlantic increased high-altitude atmospheric humidity and heavy rainfall events, but those events did not alleviate severe and long-lasting droughts. Amazonia fire risk is most significant in the southeastern region where tropical savannas undergo long seasonally dry periods. We also find that fires have been expanding through the wet–dry transition season and northward to savanna–forest transition and tropical seasonal forest regions in response to increased forest loss at the "Arc of Deforestation." Tropical forests, which have adapted to historically moist conditions, are less resilient and easily tip into an alternative state. Our results imply forest conservation and fire protection options to reduce the stress from positive feedback between forest loss, climate change, and fire.

KEYWORDS
Amazonia, climate shift, drought, fire, forest loss, savanna, seasonal forest

1 | INTRODUCTION

Amazonian forests have been under serious and increasing threats from extensive climate change, deforestation, and fires. The major concern, primarily based on global climate model simulations, is that Amazonia and its surroundings are anticipated to experience warmer and potentially drier climate (Christensen et al., 2013). The resulting climate-induced plant water stress is likely to cause forest canopy dieback and increase fire susceptibility during this century (Malhi et al., 2009). Two opposing hydrological trends that affect fire susceptibility have been observed within recent decades. First, the hydrological cycle has intensified as evidenced from increased Amazon river discharge and basin-wide precipitation in the past several decades (Gloor et al., 2013; Skansi et al., 2013). Second, in contrast, increased drought frequency and severity has been reported (Fu et al., 2013), which enhances forest flammability and suppresses tree growth (Nepstad et al., 2004).

Changes in the Amazonian hydrological cycle have been attributed to large-scale climate change, deforestation, or their interactions (Trenberth et al., 2014; Zhang et al., 2017). The intensified wet season precipitation in the last three decades coincided with a warming tropical Atlantic that increased atmospheric water vapor transport to Amazonia (Gloor et al., 2013). Strong tropical Atlantic warming and tropical Pacific cooling strength the Walker circulation, which causes wet seasons to be wetter and dry seasons to be drier (Barichivich et al., 2018). These results, and others (Espinoza, Ronchail, Marengo, & Segura, 2019), indicate that the combined impact of the tropical Pacific and Atlantic oceans on Amazonian drought is complex and is linked to phases of the El Niño-Southern Oscillation (ENSO) and the North Atlantic Oscillation (NAO; Yoon & Zeng, 2010).

Changes in hydrological dynamics in Amazonia due to deforestation have been the focus of many studies (e.g., Cavalcante, Pontes, Souza-Filho, & de Souza, 2019; Chambers & Artaxo, 2017; D'Almeida et al., 2007; Staal et al., 2020). About one-third of the moisture that forms precipitation over the Amazonia is locally supplied through recycling of evapotranspiration (Davidson et al., 2012). Deforestation causes a decline in both evapotranspiration from deforested regions and downwind transport of water vapor (Ellison et al., 2017). As a result, deforestation reduces precipitation and increases the amplitude of droughts in the region (Bagley, Desai, Harding, Snyder, & Foley, 2013). Extensive deforestation significantly alters river discharge and flood-pulse magnitude (Coe, Costa, & Soares-Filho, 2009). The loss of vegetation canopy can lead to increased runoff due to reduction in canopy interception and evapotranspiration (Clark, 1987), which increases surface runoff and amplifies flood risk and severity (Bradshaw, Sodhi, Peh, & Brook, 2007). Fragmented forests due to deforestation are prone to drought and flood damage, which exacerbates tree mortality and fire vulnerability (Laurance & Williamson, 2001).

Risks of fire increase as forests become stressed by climate change and forest loss. Shifted seasonality (Fu et al., 2013) and extreme weather and climate events (Negrón-Juárez et al., 2018; Nepstad, Tohver, David, Moutinho, & Cardinot, 2007) increase tree mortality. Trees are particularly vulnerable to repeated and prolonged droughts (Phillips et al., 2010; Taufik et al., 2017). The process of reducing live canopy fuels and increasing dead fuels influences the spread and intensity of fires (Stephens et al., 2018). Deforestation leads to increases in downed woody debris and therefore greater fuel mass (Uhl & Kauffman, 1990). Furthermore, forest fragments resulting from deforestation and agricultural expansion are fire-prone because they are often adjacent to cattle pastures and are therefore drier and warmer (Laurance et al., 2018) and more often logged and burned (Laurance & Williamson, 2001). Tree mortality due to climate change or deforestation allows sunlight to heat the forest floor and dry out litter fuel, making it more flammable (Messina & Cochrane, 2007).

Although climatic and anthropogenic threats facing Amazonian forests have caused great concern among scientific communites, current understanding of linkages between climate change and deforestation-induced hydrological changes and fire susceptibility are isolated and qualitative, based mainly on reviews of individual studies (Cochrane & Barber, 2009; Davidson et al., 2012; Malhi et al., 2008; Nobre et al., 2016). Here we use multiple satellite observations and climate reanalysis datasets to explore spatial and temporal changes in Amazonia fire regime in that experiences seasonal dry period and examine responses to climate regime shifts and forest loss.

2 | DATA AND METHODS

2.1 | Climate regime analysis

The Amazonia extends over three tropical climate zones (Figure S1a): tropical rainforest (Af), tropical monsoon (Am), and tropical winter dry (Aw) climates according to Köppen–Geiger climate classification for 1951–2000 period at 0.5 degree (Beck et al., 2018). Tropical rainforest climate is wet and humid year-round with dominant land cover of tropical rainforest. The tropical monsoon and tropical winter dry climates are characterized by contrasting wet and dry seasons. The dry and wet seasons extend over August–October and January–March, respectively, with other months transitioning between wet–dry and dry–wet seasons. The land cover in the winter dry zone is dominated by tropical savannas. Tropical seasonal forests or monsoon forests, which are in the transitional region between rainforests and savannas, dominate the tropical monsoon zone (Wright et al., 2017).

We calculated the 30-year (1961–1990) mean climate of the Am and Aw in the south of Af where Am and Aw share a similar seasonal precipitation pattern, despite precipitation gradient from the northwest to southeast across Am and Aw. Monthly total precipitation was calculated from 0.5-degree Global Precipitation Climatology Centre (GPCC) monthly precipitation dataset (Schneider et al., 2011). Monthly mean temperature was calculated from 0.5-degree GHCN_CAMS Gridded 2 m temperature (Fan & van den Dool, 2008). We defined three 3-month periods with distinctive precipitation patterns for our analysis: (a) January to March, with the highest precipitation, is the wet season; (b) August to October, with lowest precipitation, is the dry season; and (c) May to July, with gradual increases in precipitation, is the transition season (Figure S1b–e).

The 2 m air temperature, precipitation, column water vapor, vertically integrated water vapor transport, and meridional and zonal wind at 850 hpa were analyzed with European Centre for Medium-Range Weather Forecasts (ECMWF) ERA5 monthly reanalysis at 0.25-degree (ERA5, 2019). All variables were resampled to 0.5-degree using 2 × 2 0.25-degree grids to accommodate the resolution of Köppen–Geiger climate classification. The relative changes of all the variables between two periods, 1981–2000 and 2001–2018, were calculated for Am and Aw. Probability density functions (Weibull distribution) of monthly mean air temperature and monthly total precipitation were analyzed for wet, transition, and dry seasons in 1981–2000 and 2001–2018 periods. Changes in

1,000 hpa to 500 hpa relative humidity between 2001–2018 and 1981–2000 were calculated to quantify the vertical profile of moisture change.

Drought conditions in Am and Aw were analyzed with the Self-calibrating Palmer Drought Severity Index (scPDSI; Barichivich, Osborn, Harris, van der Schrier, & Jones, 2019; van der Schrier, Barichivich, Briffa, & Jones, 2013). scPDSI was calculated from precipitation and temperature time series with fixed parameters related to soil and surface characteristics at each grid cell. Dry and wet conditions were classified into 11 categories (Table S1) as defined by Palmer for the PDSI (Palmer, 1965). scPDSI in this study spanning the period 1981–2018 was calculated using CRU monthly surface climate data version CRU TS4.03 at 0.5-degree. Time series of scPDSI for wet, transition, and dry seasons in the entire Am and Aw region were calculated. The probability density functions (kernel distribution) of scPDSI were analyzed for wet, transition, and dry seasons in 1981–2000 and 2001–2018 periods.

2.2 | Biophysical impact of forest loss

The global forest change (GFC) dataset (Hansen et al., 2013) at 30-m resolution, between 2000 and 2017 provides forest cover information in 2000 and forest loss and gain for each year during the period. Forest loss and gain are defined as the transition from forest to non-forest, and non-forest to forest, respectively, by taking forest cover in 2000 as a base condition. We resampled forest cover and forest change to 0.05-degree and calculated the percent of forest cover in 2000 and accumulative forest loss since 2000 in each 0.05-degree grid.

We distinguished disturbed forests from pristine forests and compared observationally derived evapotranspiration and land surface temperatures between them for Am and Aw to explore the impact of forest loss on local temperature and water conditions. Disturbed forest and pristine forests were screened with 0.05-degree grids by a window searching method (Li et al., 2015). Disturbed forests are identified according to the following criteria: (a) forest cover (F_{cover}) in 2000 was greater than 70% and (b) the accumulated loss (F_{loss}) during 2001–2017 was greater than 65%. Pristine forest is identified according to the criteria (a) F_{cover} in 2000 was greater than 70% and (b) F_{loss} during 2000–2017 was less than 5%. We then searched 10 × 10 0.05-degree grids within each 0.5-degree grid cell with the assumption that the background climate is similar in each 0.5-degree grid cell. If disturbed and pristine forests were both present in the same 0.5-degree grid cell, this 0.5-degree grid cell is valid for comparison of the land surface temperature, water, and energy fluxes between disturbed and pristine forests to analyze biophysical impacts of forest loss. As a result, 33 grid cells for Am and 183 grids for Aw were used to calculate the biophysical impacts of forest loss.

We used Moderate Resolution Imaging Spectroradiometer (MODIS) Aqua 8-day Land Surface Temperature and Emissivity (LST&E) L3 Global products (MYD11C2 Version 6; Wan, Hook, & Hulley, 2015) to quantify the land surface temperature changes due to forest loss. MYD11C2 is configured on a 0.05-degree latitude/longitude climate modeling grid.

MODIS Bidirectional Reflectance Distribution Function and Albedo (BRDF/Albedo) dataset (MCD43C3 Version 6; Schaaf & Wang, 2015) was used to quantify albedo changes due to forest loss. MCD43C3 is produced daily using 16 days of Terra and Aqua MODIS data in a 0.05-degree Climate Modeling grid. MCD43C3 provides black-sky albedo (directional hemispherical reflectance) and white-sky albedo (bihemispherical reflectance) at local solar noon. Actual clear sky albedo (blue-sky albedo) is calculated as the mean of black-sky and white-sky albedo because of their small differences and high correlation (Li et al., 2015).

We used the MODIS evapotranspiration and latent heat flux product (MOD16A2 Version 6; Running, Mu, & Zhao, 2017) of 8-day temporal resolution and 500 m spatial resolution to quantify evapotranspiration changes due to forest loss. MOD16A2 collection is derived based on the logic of the Penman–Monteith equation using daily meteorological reanalysis data with MODIS vegetation property dynamics, albedo, and land cover. We resampled MOD16A2 from 500 m to 0.05-degree using bilinear interpolation provided by MODIS reprojection tool.

We assume the background climate is similar in each 0.5-degree grid so that the temperature and energy fluxes difference in disturbed (D) and pristine (P) 0.05-degree grids in the same 0.5-degree grid is caused by the forest loss. The land surface temperature change (ΔLST) due to accumulated forest loss was calculated as the difference of LST in disturbed forest grids (LST_D) and LST in pristine forest grids (LST_P) in 2017,

$$\Delta LST = LST_D - LST_P. \quad (1)$$

ΔLST was calculated with MODIS Aqua 8-day LST&E L3 Global products (MYD11C2 Version 6).

The evapotranspiration change (ΔET), latent heat change (ΔLE), and albedo change (ΔAlbedo) due to accumulated forest change were calculated following the same way as LST,

$$\Delta ET = ET_D - ET_P, \quad (2)$$

$$\Delta LE = LE_D - LE_P, \quad (3)$$

$$\Delta Albedo = Albedo_D - Albedo_P. \quad (4)$$

The subscripts D and P denote the disturbed and pristine forest grids, respectively. ΔET and ΔLE were calculated with MODIS evapotranspiration and latent heat flux product (MOD16A2 V6). ΔAlbedo was calculated from Equation (4) with MODIS BRDF/Albedo dataset (MCD43C3 V6).

The surface shortwave net radiation change (ΔSSNR) between disturbed and pristine forest grids was calculated as,

$$\begin{aligned}\Delta SSNR &= (1 - Albedo_D) \times S_{in} - (1 - Albedo_P) \times S_{in} \\ &= -\Delta Albedo \times S_{in}, \end{aligned} \quad (5)$$

where S_{in} is the downward shortwave radiation from Clouds and the Earth's Radiant Energy System (CERES) Energy Balanced And Filled (EBAF) Surface Product. Under clear sky conditions, S_{in} is assumed homogeneously distributed in the 0.5-degree grid.

2.3 | Fire regime analysis

We used two burn area (BA) datasets to analyze the spatial and temporal variation of fire BA within and across the south boundary of Amazon basin. The ESA Fire Climate Change Initiative (Fire CCI) Dataset Collection (Otón, Ramo, Lizundia-Loiola, & Chuvieco, 2019) is generated from Advanced Very High Resolution Radiometer images under the land long-term data record project. Fire CCI spans from January 1982 to December 2017 with monthly resolution. BA in 1994 was excluded due to data quality issues. The spatial resolution of Fire CCI is 0.05-degree. Global Fire Emissions Database, Version 4.1 (GFEDv4; Randerson, van der Werf, Giglio, Collatz, & Kasibhatla., P. S., 2018) provides monthly burned area (Ba) over June 1995–December 2016 of 0.25-degree spatial resolution. We integrated the total BA in each 0.5-degree for Fire CCI (10 × 10 0.05-degree) and GFEDv4 (2 × 2 0.25-degree) to accommodate the spatial resolution of Köppen–Geiger climate classification and other climate reanalysis data. The 1982–2017 annual mean fraction of Ba and monthly mean Ba were plotted with Fire CCI. We used GFEDv4 from January 2001 to December 2016, to compare burned fraction and area with that by Fire CCI. Fire CCI and GFEDv4 showed comparative spatial pattern and Ba during 2001–2016 (Table S2).

The annual mean Ba in 2001–2017 is compared with that in 1982–2001 to examine the spatial pattern of Ba change in dry and

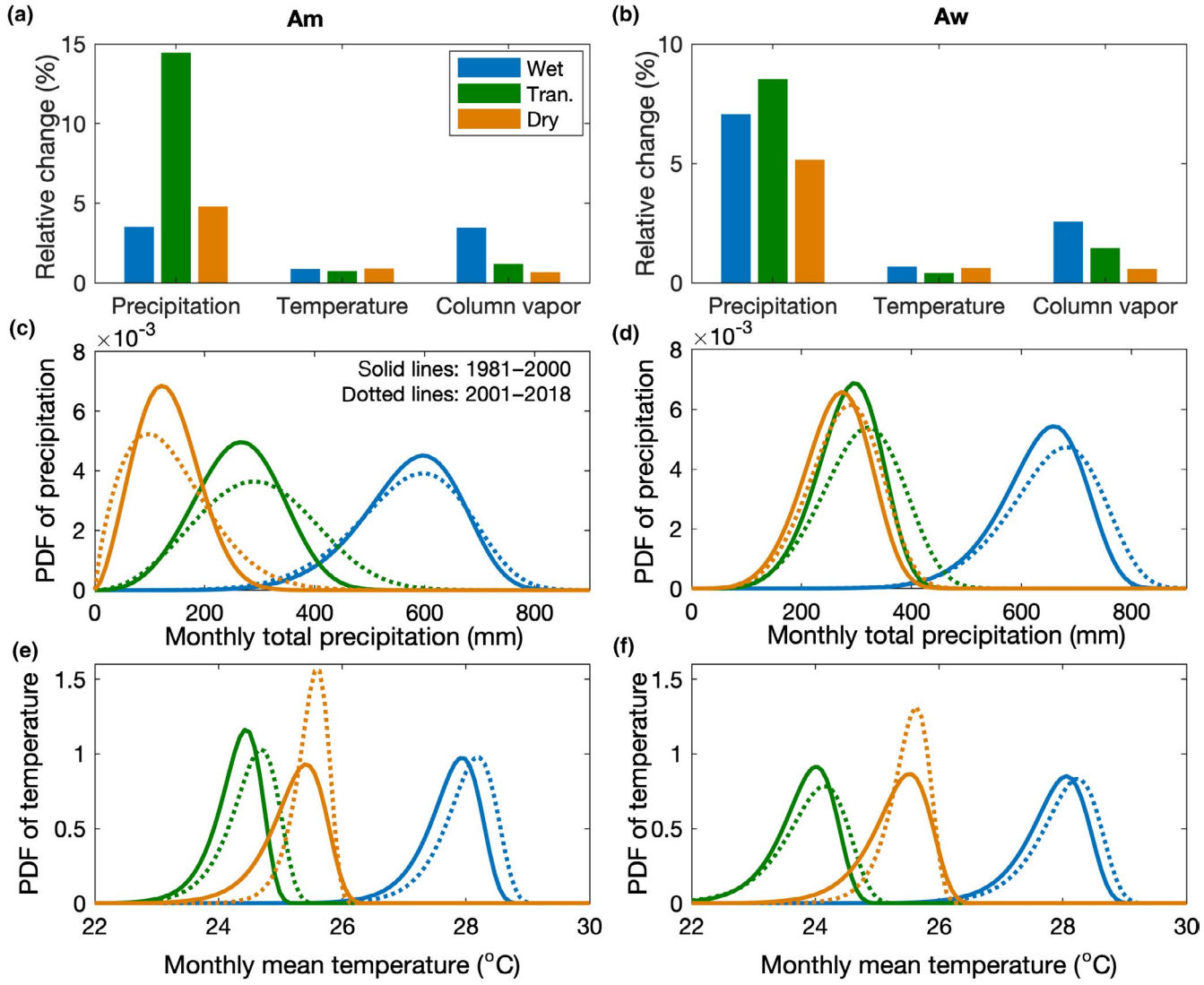

FIGURE 1 Climate regime shift of Amazon monsoon (Am) and winter dry (Aw) climates. The relative change (%) of precipitation, temperature, and total column water vapor during 2001–2018 relative to that in 1981–2000 for Am (a) and Aw (b), probability distribution functions of precipitation for Am (c) and Aw (d), and probability distribution functions of temperature for Am (e) and Aw (f) for wet season, transition season and dry season. The solid and dotted lines in (c–f) denote probability distribution functions for precipitation (c and d) and temperature (e and f) in 1981–2000 and 2001–2018, respectively

transition season. The number of grid cell with increased Ba ($\Delta Ba > 0$) and disturbed forest is counted to evaluate the tendency of burning with forest loss. We further classify the forest loss fraction to four levels, that is, 0%–10%, 10%–20%, 20%–30%, 30%–40%, and >40% to identify the probability of increased BA.

3 | RESULTS

3.1 | Decadal climate regime shift to intensified climate extremes

In the past four decades, Amazonian climate has experienced abrupt changes. Mean monthly precipitation after 2001 increased by 3.3%–14.5% in different seasons and climate zones compared to that during 1981–2000 (Figure 1a,b). The increased precipitation coincided with higher total column moisture content, which is consistent with enhanced water vapor transport from the tropical Pacific to the whole basin in the wet season and from the tropical Atlantic to southeastern Amazonia in the transition and dry seasons (Figure 2) between 2001 and 2018. In both Am and Aw, enhanced precipitation was mainly in the form of intensified precipitation (Figure 1d). In Am, low precipitation frequency and rain-free days also increased, particularly in the dry season.

The increased frequency of extremely low and high precipitation was accompanied by warming in Am and Aw, with near-surface air temperatures (2 m temperature) rising at about ~0.10°C per decade and ~0.12°C per decade, respectively. As a result, annual mean air temperature in the recent two decades (2001–2018) was about 0.20°C higher in Aw and 0.24°C higher (increased by 0.90%) in Am, compared to 1981–2000. The warming in both Am and Aw was mainly contributed by increased occurrence of high temperatures in the wet and transition seasons, while in the dry season the warming was mainly due to decreased occurrence of low temperatures (Figure 1e,f).

The shifted seasonal temperature and precipitation distributions coincided with more extremely dry and wet conditions in Am and Aw despite the increased total precipitation and column water vapor content. The drought severity and extent both increased according to the scPDSI (Barichivich et al., 2019; van der Schrier et al., 2013; Figure 3). The regional mean scPDSI over the periods 1999–2004 and 2009–2015 indicated sustained drought conditions (scPDSI < −0.5; Figure 3a–c). On average, the areal extent of (a) normal and near-normal drought conditions (−1 < scPDSI < 1) have been decreasing at 2.0%–4.8% per

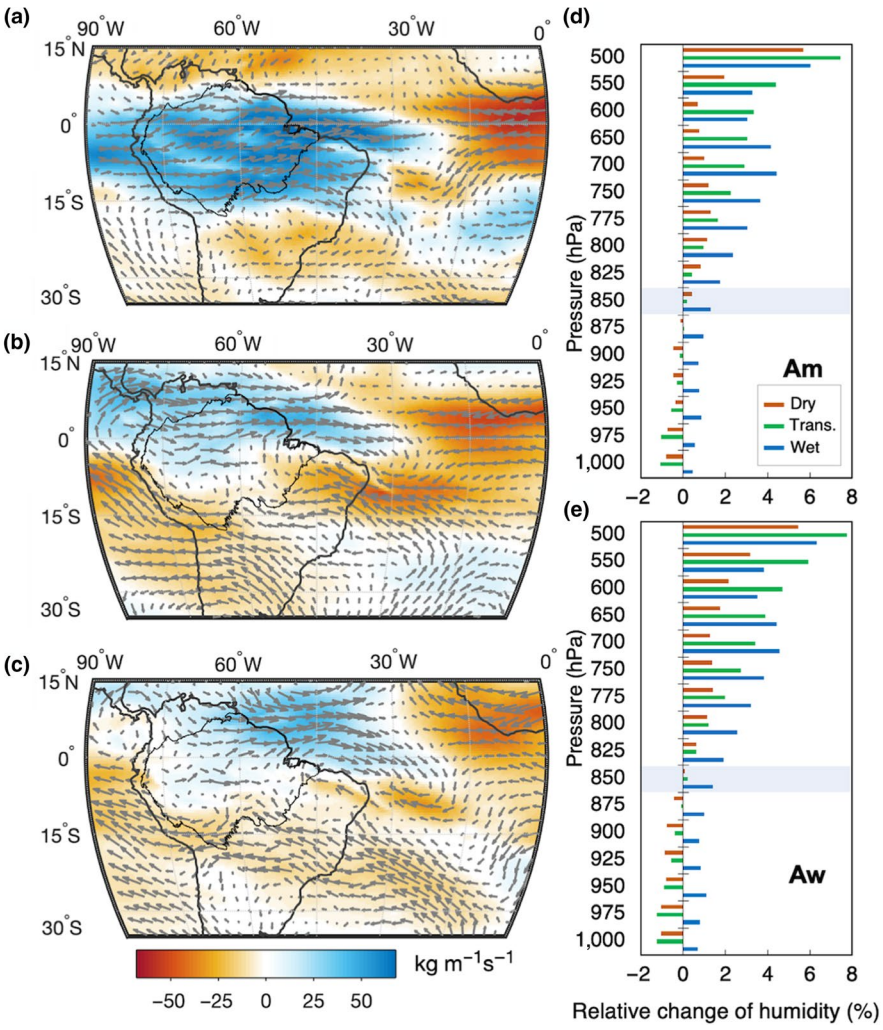

FIGURE 2 Changes in vertically integrated eastward water vapor fluxes and vertical profiles of water vapor change. Vertically integrated eastward water vapor fluxes ($kgm^{-1}\ s^{-1}$) change in 2000–2018 in relative to 1981–2000 for (a) dry season, (b) transition season and (c) wet season. The vertical profiles of relative change (%) in specific humidity between 2001–2018 and 1981–2000 for wet, transition, and dry season in tropical monsoon climate region (d) and tropical winter dry climate region (e). The vectors in (a)–(c) denote the horizontal wind change between 1981–2000 and 2001–2018 at 850 hpa. The height of 850 hpa is shaded in (d) and (e). The water vapor fluxes and vertical profiles were plotted with ERA5 monthly reanalysis

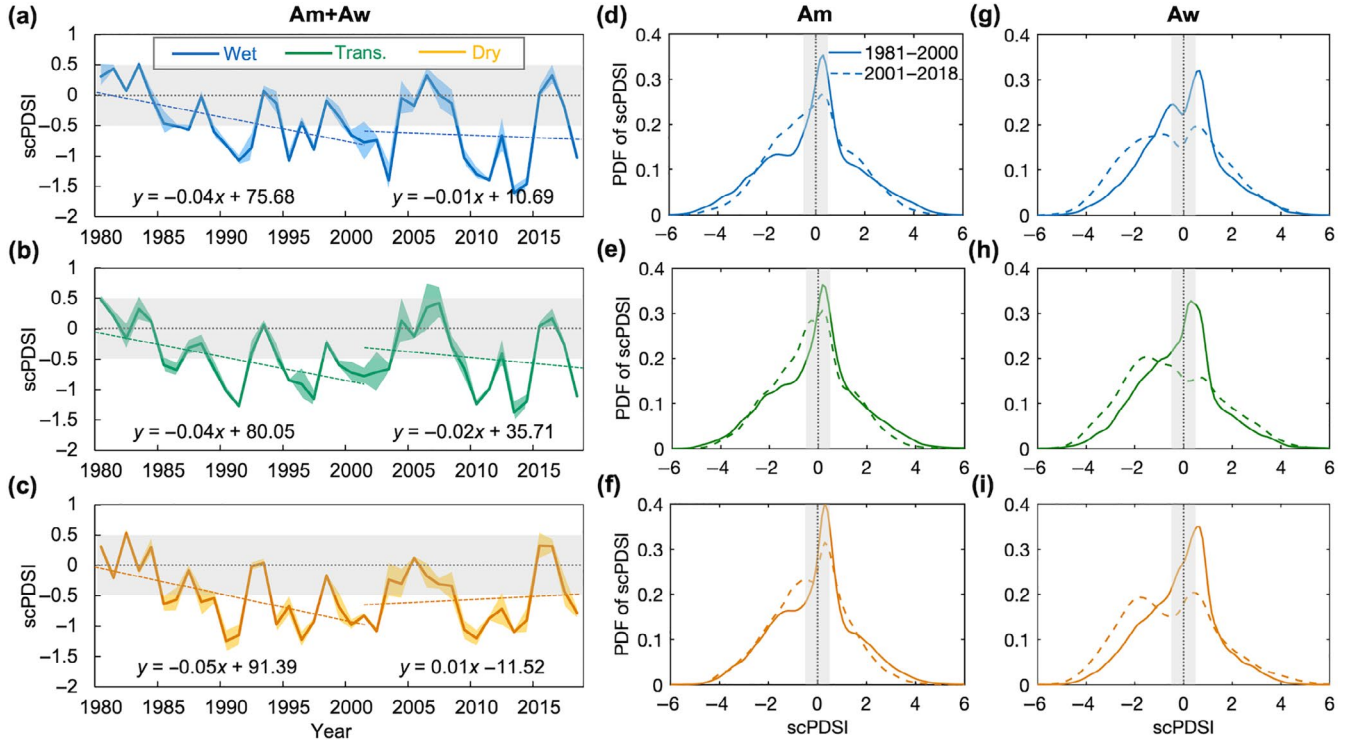

FIGURE 3 Drought conditions between 1980 and 2018 across the tropical monsoon climate and winter dry climate regions. Time series of self-calibrating Palmer Drought Severity Index (scPDSI) in wet (a), transition (b), and dry (c) seasons and the probability distribution functions of scPDSI in the wet, transition, and dry season for tropical monsoon climate region (d–f) and tropical winter dry climate region (g–i). The shaded pattern surrounding the time series (a–c) denote the standard deviation of scPDSI in each season. The solid and dashed lines in (d)–(i) denote the period 1981–2000 and 2001–2018, respectively. The grey shaded regions in (a)–(i) denote near-normal dryness condition (−0.5 < scPDSI < 0.5)

decade ($p < .001$), (b) slight to extremely dry conditions (scPDSI < −1) have been increasing at 1.9%–4.9% per decade ($p \leq .01$), and (c) slightly to extremely wet conditions (scPDSI > 1) have been increasing at 0.7%–1.7% per decade (insignificant, $0.4 < p < .9$; Figure S2). Over the four decades, drought conditions became more severe in dry and transition seasons and extended into wet and transition seasons.

Between 1981 and 2000, the seasonal scPDSI probability distribution function had regular unimodal patterns, that is, mean water availability in all seasons was near normally distributed with a peak toward being slightly wet (0.3 < scPDSI < 0.7). However, the scPDSI pattern evolved to be more bimodal after 2000, mainly due to increased occurrence of drought. The near-normal condition (−0.5 < scPDSI < 0.5) shifted to more dry conditions (−2 < scPDSI < −0.5) in Am, and moderately dry and extremely dry conditions in Aw (scPDSI < −2; Figure 3d–i). In Aw, droughts in transition and dry seasons expanded to a larger area. Even in the wet season, moderate and extreme droughts increased significantly.

3.2 | Warmer and drier lower atmosphere due to forest loss

The Amazonia has experienced intensive forest loss due to deforestation, climate change, and fire. Since the 20th century, reduction in forest cover mainly occurred at "Arc of Deforestation" (Malhi et al., 2008) in eastern and southern Amazonia (Figure 4a). The forest loss rates across Af, Am, and Aw have been estimated to be $47.8 \pm 14.9 \times 10^3$ km^2/year during 2001–2017, in which 11.9 ± 3.5% of the losses were in tropical rainforest, 23.5 ± 3.2% in tropical seasonal forest, and 64.6 ± 5.3% in tropical savannas according to the GFC dataset.

Accumulated forest loss during 2000–2017 resulted in a decline in ET (Figure 4b,c). Annual ET decreased by −76.1 ± 80.5 mm/year and −213.3 ± 88.1 mm/year for Am and Aw, respectively. The decreased ET occurred across the transition and dry seasons, with maximum decreases in August for Am (−34.9 ± 20.1 mm/month) and Aw (−36.8 ± 20.1 mm/month), respectively. A direct impact of declining ET is reduced atmospheric specific humidity. The observational reanalysis record is consistent with this effect, with the atmosphere drying to an altitude corresponding to 875–850 hpa in transition and dry seasons (Figure 2d,e). The near-surface (i.e., below 850 hpa) mean humidity in the transition and dry seasons over 2001–2018 decreased by 0.91% and 1.15% for Am and Aw, respectively, relative to 1981–2000.

ET requires a substantial amount of energy to vaporize water. ET reductions not only limit water vapor contributions to the lower atmosphere, thereby reducing moisture buffering of temperature changes, but also substantially diminishing surface latent heating. The forest loss caused reductions in annual mean latent heat

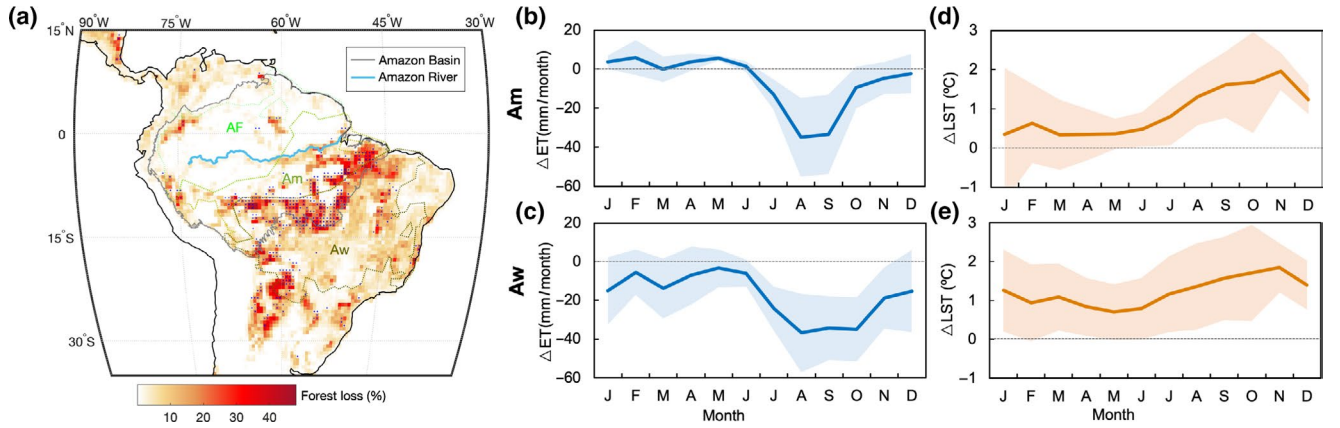

FIGURE 4 Forest loss and affected regional evapotranspiration and land surface temperature. Accumulative forest loss (Floss, %) during 2000–2017 in each 0.5 × 0.5° grid cell according to the global forest change dataset (a), the blue dots denote the grid cells with both large forest loss (Floss > 65%) and pristine forest (Floss < 5%) between 2001 and 2017, monthly evapotranspiration change (ΔET, mm/month) due to accumulated forest loss in Am (b) and Aw (c), and monthly mean land surface temperature change (ΔLST, °C) due to accumulated forest loss in Am (d) and Aw (e). The shaded patterns in (b)–(e) are standard deviation of ΔET and ΔLST in grid cells with both large forest loss (Floss > 65%) and pristine forest (Floss < 5%) between 2000 and 2017

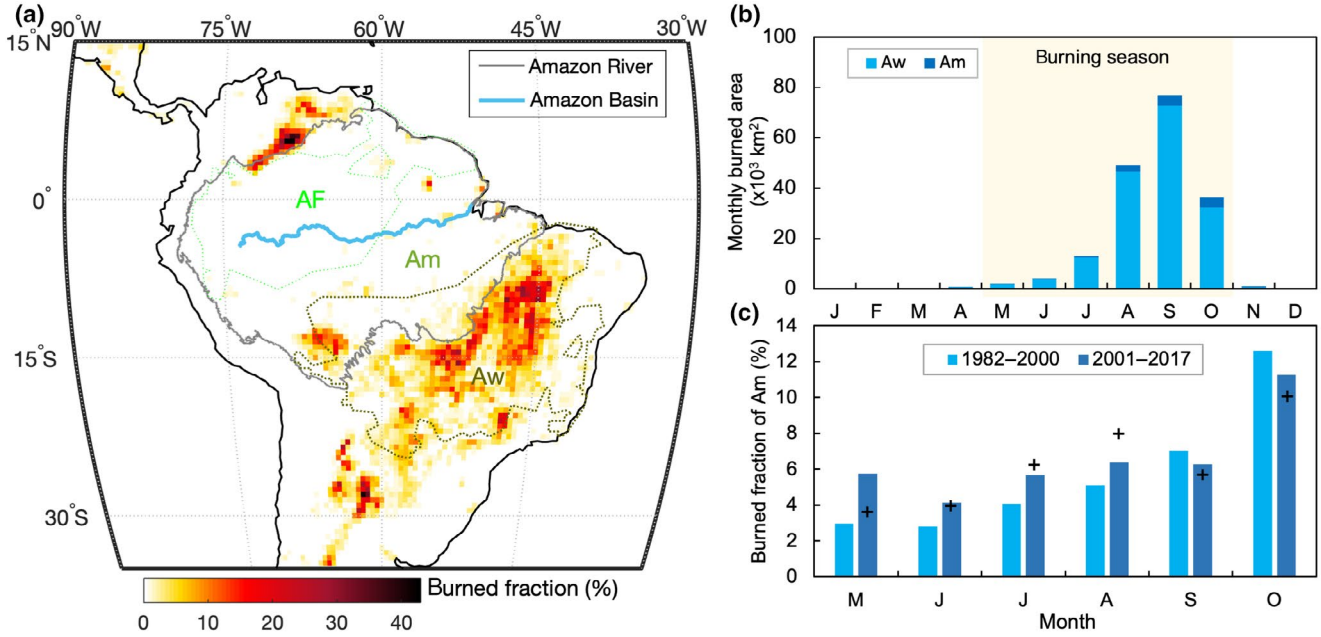

FIGURE 5 The spatial and seasonal distribution of fire in Amazonia. The annual mean fraction of fire burn in Amazon region between 1982 and 2017 based on ESA Fire Climate Change Initiative (Fire CCI) Dataset Collection (a). The dotted lines denote the major boundaries of Köppen-Geiger climate zones of tropical rainforest (Af), tropical monsoon climate (Am), and tropical winter dry climate (Aw). The mean seasonal distribution of burned area in tropical monsoon region (Am) and tropical winter dry region (Aw) during 1982–2017 (b) and the fraction of burned area in Am and Aw that occurred in Am between May and October during 1982–2000 and 2001–2017 periods (c). The black + symbols in (c) denote the fraction of burned area in Am over the entire Am and Aw regions between May and October during 2001–2016 calculated from Global Fire Emissions Database, Version 4.1 (GFEDv4)

between 2001 and 2017 of −5.9 ± 6.3 W/m^2 and −16.6 ± 6.8 W/m^2 in Am and Aw, respectively. The seasonal pattern of latent heat changes due to forest loss was similar to that of ET, with major reductions in the transition and dry seasons, and maximum reductions in August of −31.8 ± 18.4 W/m^2 and −33.7 ± 18.4 W/m^2 for Am and Aw, respectively (Figure S3a,b).

The surface warming impacts of reduced latent heating can be partially offset by the cooling impacts of forest loss induced surface albedo change. Accumulated forest loss increased surface albedo in 2001–2017, thereby decreasing annual mean SSNR by −5.8 ± 1.7 W m^{-2} and −7.2 ± 1.6 W m^{-2} for Am and Aw, respectively. This cooling impact is lower in the dry season when the forest canopy is sparser than in the

wet season (Figure S3c,d) and can also be reduced by decreasing cloud cover (and thereby reduced ET; Bala et al., 2007). The tropical forest loss induced ET and albedo changes and their subsequent cloud and greenhouse gas feedbacks have a net warming impact at the regional scale (Figure 4d,e). The accumulated forest loss between 2001 and 2017 was coincident with an annual mean LST change of 0.9 ± 0.5°C and 1.2 ± 0.7°C for Am and Aw, respectively. The warming is most significant in the dry season from August to November.

3.3 | Fire expansion due to climate shift and forest loss

The fire Ba across Amazonia is mainly distributed across the southern boundary of the Amazon basin in Am and Aw (Figure 5a). Between 1982 and 2017, ~93% of the mean annual Ba occurred in Aw and ~94% of fires occurred in the dry season with peak burn from August to October (Figure 5b). Despite interannual variation, the annual total Ba (178.5 ± 65.4 × 10^3 km^2) in Am and Aw was relatively stable between 1982 and 2017. The Ba in Am expanded between 2001 and 2017 relative to between 1982 and 2000. The expanded burn occurred mainly in the transition season between May and August, when the mean fraction of Ba in Am increased from 3.7 ± 3.7% (1982–2000) to 5.4 ± 3.4% (2001–2017) with a maximum increase in May (about doubling; Figure 5c).

The disturbed forests in the transition season are more prone to burning than in wet and dry seasons. In the transition season, 72% of Aw and 68% of Am (compared to 53% of Aw and 47% of Am in dry season) disturbed forests showed fire increases during 2001–2017, compared to during 1982–2000. The Ba increased mainly across the southern boundary of the Amazon basin at "Arc of Deforestation" (Figure S4). However, the Ba decreased in the southern Aw where the climate is much drier and experienced a more intensive drying trend than in Am and northern Aw. Compared to the dry season, transition season fires clearly expanded within and across the southern boundary of the basin where forests are highly disturbed. The fraction of increased Ba is largely dependent on the fraction of forest loss (Figure 6). The increased burn rates are higher in the transition seasons than in the dry seasons, particularly in the seasonal forests. Furthermore, the seasonal forests had obvious increases in fires in response to forest loss, while responses to increased tree losses in savannas were relatively stable.

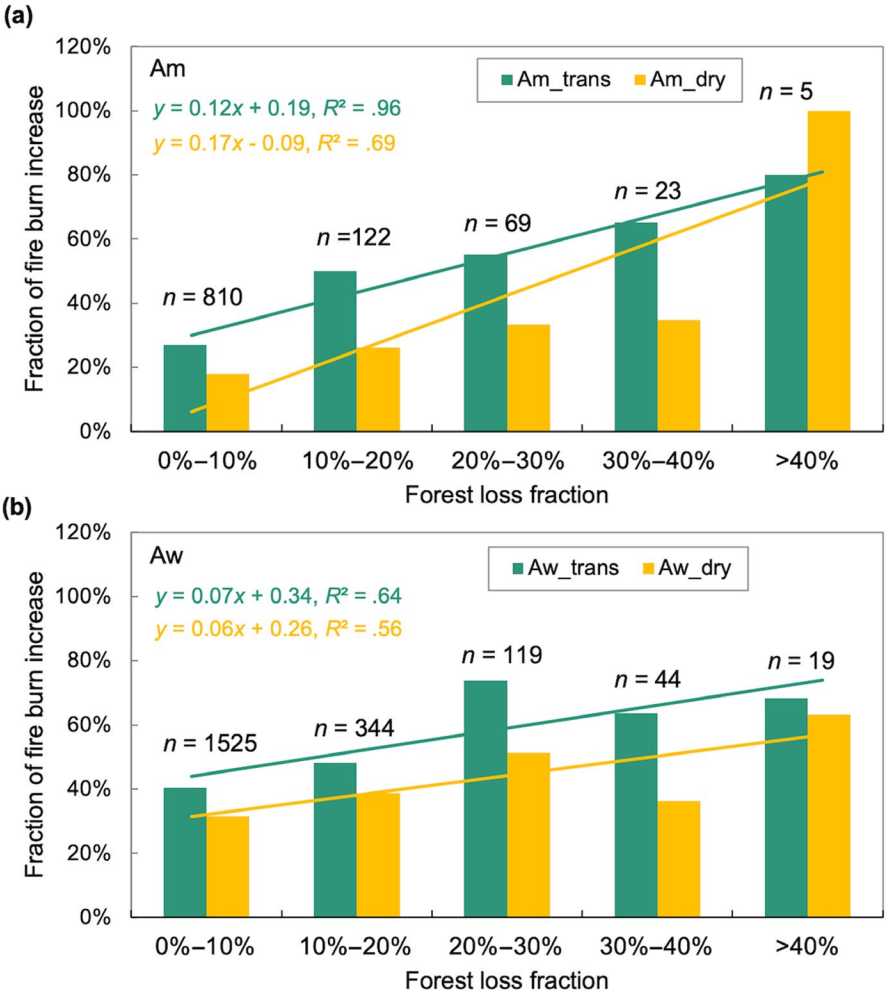

FIGURE 6 Fraction of burned area increase is largely dependent on the fraction of forest loss. (a) Fraction of increased burned area against fraction of forest loss in tropical monsoon region (Am) for transitional and dry seasons and (b) fraction of burned area increase against fraction of forest loss in tropical winter dry region (Aw) for transitional and dry seasons. *n* is the total number of grid cells for each category of forest loss fraction

4 | DISCUSSION

The Atlantic Ocean supplies two-thirds of Amazonia precipitation (Davidson et al., 2012). Amazonia wetting in recent decades has been attributed to increasing atmospheric water vapor transport from the warming tropical Atlantic (Gloor et al., 2013). Water vapor transport from the tropical Atlantic to southeastern Amazonia in the transition and dry seasons was enhanced between 2001 and 2018, which can explain the increased precipitation and moisture in savannas. While in seasonal forests, the increased precipitation and moisture were contributed by enhanced water vapor transport from the tropical Pacific. Enhanced water vapor transport from the tropical Pacific in the wet season is consistent with the basin-wide wetting.

Increased precipitation occurred mostly in intensified heavy rainfall events. This shifted precipitation pattern of intensified heavy rainfall events and extremely wet days has been observed since the mid-20th century (Skansi et al., 2013). Our results showed increased low precipitation frequency and rain-free days, and enhanced drought severity and extent, particularly in seasonal forests, indicating polarization between extreme precipitation and water stress. The increased wet and dry extremes exacerbate vulnerability and mortality of vegetation (Hirota, Holmgren, Van Nes, & Scheffer, 2011). The intensified heavy rainfall events cannot effectively ease or alleviate long-lasting drought because most of that rainfall runs off into drainage channels and streams rather than being absorbed into the ground (Trenberth et al., 2014). Furthermore, runoff from heavy rainfall events is enhanced in regions of vegetation loss because of reduced rainfall interception, canopy evapotranspiration, and soil infiltration, amplifying flood risk (Bradshaw et al., 2007; Gentry & Lopez-Parodi, 1980; Lawrence & Vandecar, 2015).

In Amazonia, forest moisture and thermal conditions are largely driven by tropical Pacific and Atlantic sea surface temperatures (SST) that fluctuate with the ENSO and NAO phases (Jiménez-Muñoz et al., 2016; Zeng et al., 2008). However, some drought events cannot be fully explained by SST anomalies, for example, the 2015–2016 unprecedented drought (Erfanian, Wang, & Fomenko, 2017). Our results showed that the decreased ET due to forest loss dries the lower atmosphere and likely amplifies drought severity, particularly in tropical savannas. Savanna soils tend to be porous with more rapid drainage than in tropical seasonal forests (Lloyd et al., 2009). Therefore, even in the wet season, tree loss in savannas reduces ET due to low soil water-holding ability. The large decline in ET implies a substantial reduction in water supply to the lower atmosphere since ET accounts for ~1/3rd of Amazonia rainfall (Staal et al., 2018) and ~90% vapor content in near-surface subcanopy layer (Cochrane & Barber, 2009).

The contrasting change of specific humidity in the low- and high-level atmosphere implies differences in water supply mechanisms. Increased humidity at all levels in the wet season and upper atmosphere in the transition and dry seasons is consistent with enhanced precipitation and column water vapor content and are more likely explained by increased water vapor transport from the tropical oceans as we found. The level of decreased specific humidity occurs right below 850 hpa, the level at which a large proportion of moisture is conveyed from oceans (Gimeno et al., 2016). However, the drying lower-level atmosphere is consistent with reduced ET because ET is the major moisture source in the Amazonian low atmosphere (Cochrane & Barber, 2009), which implies a substantial weakening of atmospheric moisture recycling due to forest loss. The decreased moisture recycling due to forest cover loss can substantially delay the initiation of dry-to-wet season transitions (Wright et al., 2017) and extend the dry season (Agudelo, Arias, Vieira, & Martínez, 2019).

The spatial gradient of fire from northwest to southeast is related to climate patterns and forest distribution. The high humidity and canopy water content make the northwest Amazonian rainforest extremely resistant to fire spread (Cochrane & Barber, 2009). However, savannas in the southern and eastern Amazonia, which experience seasonal rainfall, are not effectively buffered from fire (Uhl, 1998). Savannas are naturally fire-prone and adapted to frequent fire. Therefore, we found that as the forest loss rate increases, the fire BA stays relatively stable. Fire risk in seasonal forests is generally much lower than surrounding savannas because of less-open canopy, lower mass of fuel, and higher litter moisture (Bowman & Wilson, 1988).

Our results indicated that seasonal forests and the forests across the seasonal forest-savanna boundary experienced much higher losses than northern rainforests and southern savannas and are more susceptible to fire. Fires increased in more than half of the regions which experienced forest cover losses larger than 10%. More than 80% of the regions where forest cover losses greater than 40% experienced increases in fire. Forest canopy loss reduces forest fuel moisture in the subcanopy and allows solar radiation to heat understory vegetation and dry litter fuel (Messina & Cochrane, 2007). Forest loss due to either natural or anthropogenic activities causes fragmentation, leading to ignition increases and fuel moisture decreases (Alencar, Brando, Asner, & Putz, 2015). Forest fragments are particularly vulnerable and fire-prone because they are often adjacent to cattle pastures which are often logged and burned (Laurance & Williamson, 2001).

We showed that forest loss modifies regional climate, and when superimposed on climate change, can increase fire susceptibility and exacerbate regional drought. Intensive drought interactions with fire cause large-scale changes to canopy structure and composition, and shifts forest to savanna-like or scrub vegetation (Balch et al., 2008; Hutyra et al., 2005).The savanna-like vegetation is more flammable yet better fire adapted. Repeated droughts that persist for years can cause vegetation mortality and amplify forest losses (Brando et al., 2014; Saatchi et al., 2013; Zemp et al., 2017). The rising deforestation rate in recent years (Qin et al., 2019) potentially increases droughts, forest fragments, and fire loads, and therefore expands fire risk northward to the tropical seasonal forest. Efforts to promote forest conservation and fire protection is a critical priority to prevent Amazonia from further climate and fire regime shift that compromises regional sustainability.

ACKNOWLEDGEMENTS

X.X., X.Z., and Y.X. were supported by the Natural Science Foundation of China (#41875107) and National Key R&D Program of China (2018YFA0606002). G.J. was supported by Strategic Priority Research Program of the Chinese Academy of Sciences, CASEarth (XDA19030401). W.J.R. was supported by U.S. Department of Energy, Office of Science, Biological and Environmental Research, Regional and Global Climate Modeling Program through the RUBISCO Scientific Focus Area under contract DE-AC02-05CH11231 to Lawrence Berkeley National Laboratory.

CONFLICT OF INTEREST

The authors declare no conflict of interest.

DATA AVAILABILITY STATEMENT

All reanalyses and satellite data used in this study are publicly available under the following URLs.

- GFEDv4:
https://daac.ornl.gov/VEGETATION/guides/fire_emissions_v4_R1.html
- ESA Fire CCI Dataset Collection:
https://catalogue.ceda.ac.uk/uuid/4f377defc2454db9b2a6d032abfd0cbd
- GFC (v1.5):
https://earthenginepartners.appspot.com/science-2013-global-forest/download_v1.5.html
- MODIS Aqua 8-day LST&E L3 Global products:
https://ladsweb.modaps.eosdis.nasa.gov/missions-and-measurements/products/MYD11C2/
- MODIS BRDF/Albedo dataset (MCD43C3 Version 6):
https://lpdaac.usgs.gov/products/mcd43c3v006/
- MODIS evapotranspiration and latent heat flux product (MOD16A2 Version 6):
https://lpdaac.usgs.gov/products/mod16a2v006/
- CERES EBAF-Surface Product:
https://ceres.larc.nasa.gov/products-info.php?product=EBAF
- MODIS Aqua 8-day LST&E L3 Global products (MYD11C2 Version 6):
https://lpdaac.usgs.gov/products/myd11c2v006/
- Köeppen-geiger climate classification at half-degree:
http://koeppen-geiger.vu-wien.ac.at/present.htm
- 0.5-degree GPCC monthly precipitation dataset:
https://psl.noaa.gov/data/gridded/data.gpcc.html
- 0.5-degree GHCN_CAMS Gridded 2m temperature:
https://www.esrl.noaa.gov/psd/data/gridded/data.ghcncams.html
- ECMWF ERA5 monthly reanalysis at 0.25-degree:
https://www.ecmwf.int/en/forecasts/datasets/reanalysis-datasets/era5
- Half-degree scPDSI:
https://crudata.uea.ac.uk/cru/data/drought/

ORCID

Xiyan Xu https://orcid.org/0000-0003-2732-1325
Gensuo Jia https://orcid.org/0000-0001-5950-9555

REFERENCES

Agudelo, J., Arias, P. A., Vieira, S. C., & Martínez, J. A. (2019). Influence of longer dry seasons in the Southern Amazon on patterns of water vapor transport over northern South America and the Caribbean. *Climate Dynamics*, *52*(5), 2647–2665. https://doi.org/10.1007/s00382-018-4285-1

Alencar, A. A., Brando, P. M., Asner, G. P., & Putz, F. E. (2015). Landscape fragmentation, severe drought, and the new Amazon forest fire regime. *Ecological Applications*, *25*(6), 1493–1505. https://doi.org/10.1890/14-1528.1

Bagley, J. E., Desai, A. R., Harding, K. J., Snyder, P. K., & Foley, J. A. (2013). Drought and deforestation: Has land cover change influenced recent precipitation extremes in the Amazon? *Journal of Climate*, *27*(1), 345–361. https://doi.org/10.1175/JCLI-D-12-00369.1

Bala, G., Caldeira, K., Wickett, M., Phillips, T. J., Lobell, D. B., Delire, C., & Mirin, A. (2007). Combined climate and carbon-cycle effects of large-scale deforestation. *Proceedings of the National Academy of Sciences of the United States of America*, *104*(16), 6550–6555. https://doi.org/10.1073/pnas.0608998104

Balch, J. R. K., Nepstad, D. C., Brando, P. M., Curran, L. M., Portela, O., de Carvalho, O., & Lefebvre, P. (2008). Negative fire feedback in a transitional forest of southeastern Amazonia. *Global Change Biology*, *14*(10), 2276–2287. https://doi.org/10.1111/j.1365-2486.2008.01655.x

Barichivich, J., Gloor, E., Peylin, P., Brienen, R. J. W., Schöngart, J., Espinoza, J. C., & Pattnayak, K. C. (2018). Recent intensification of Amazon flooding extremes driven by strengthened Walker circulation. *Science Advances*, *4*(9), eaat8785. https://doi.org/10.1126/sciadv.aat8785

Barichivich, J., Osborn, T. J., Harris, I., van der Schrier, G., & Jones, P. D. (2019). Drought [in "State of the Climate in 2018"]. *Bulletin of the American Meteorological Society*, *100*, S39–S40. https://doi.org/10.1175/2019BAMSStateoftheClimate.1

Beck, H. E., Zimmermann, N. E., McVicar, T. R., Vergopolan, N., Berg, A., & Wood, E. F. (2018). Present and future Köppen-Geiger climate classification maps at 1-km resolution. *Scientific Data*, *5*, 180214. https://doi.org/10.1038/sdata.2018.214

Bowman, D. M. J. S., & Wilson, B. A. (1988). Fuel characteristics of coastal monsoon forests, northern territory, Australia. *Journal of Biogeography*, *15*(5/6), 807–817. https://doi.org/10.2307/2845341

Bradshaw, C. J. A., Sodhi, N. S., Peh, K. S. H., & Brook, B. W. (2007). Global evidence that deforestation amplifies flood risk and severity in the developing world. *Global Change Biology*, *13*(11), 2379–2395. https://doi.org/10.1111/j.1365-2486.2007.01446.x

Brando, P. M., Balch, J. K., Nepstad, D. C., Morton, D. C., Putz, F. E., Coe, M. T., … Soares-Filho, B. S. (2014). Abrupt increases in Amazonian tree mortality due to drought-fire interactions. *Proceedings of the National Academy of Sciences of the United States of America*, *111*(17), 6347–6352. https://doi.org/10.1073/pnas.1305499111

Cavalcante, R. B. L., Pontes, P. R. M., Souza-Filho, P. W. M., & de Souza, E. B. (2019). Opposite effects of climate and land use changes on the annual water balance in the Amazon arc of deforestation. *Water Resources Research*, *55*(4), 3092–3106. https://doi.org/10.1029/2019WR025083

Chambers, J. Q., & Artaxo, P. (2017). Deforestation size influences rainfall. *Nature Climate Change*, *7*(3), 175–176. https://doi.org/10.1038/nclimate3238

Christensen, J. H., Kumar, K. K., Aldrian, E., An, S.-I., Cavalcanti, I. F. A., de Castro, M., … Zhou, T. (2013). Climate phenomena and their relevance for future regional climate change. In T. F. Stocker, D. Qin, G.-K. Plattner, M. Tignor, S. K. Allen, J. Boschung, & P. M. Midgley (Eds.), *Climate change 2013: The physical science basis. Contribution of working group I to the fifth assessment report of the Intergovernmental Panel on Climate Change*, (pp. 1217–1308). Cambridge, UK and New York, NY: Cambridge University Press.

Clark, C. (1987). Deforestation and floods. *Environmental Conservation*, *14*(1), 67–69. https://doi.org/10.1017/S0376892900011127

Cochrane, M. A., & Barber, C. P. (2009). Climate change, human land use and future fires in the Amazon. *Global Change Biology*, *15*(3), 601–612. https://doi.org/10.1111/j.1365-2486.2008.01786.x

Coe, M. T., Costa, M. H., & Soares-Filho, B. S. (2009). The influence of historical and potential future deforestation on the stream flow of the Amazon River – Land surface processes and atmospheric feedbacks. *Journal of Hydrology*, *369*(1), 165–174. https://doi.org/10.1016/j.jhydrol.2009.02.043

D'Almeida, C., Vörösmarty, C. J., Hurtt, G. C., Marengo, J. A., Dingman, S. L., & Keim, B. D. (2007). The effects of deforestation on the hydrological cycle in Amazonia: A review on scale and resolution. *International Journal of Climatology*, *27*(5), 633–647. https://doi.org/10.1002/joc.1475

Davidson, E. A., de Araújo, A. C., Artaxo, P., Balch, J. K., Brown, I. F., Bustamante, M. M. C., … Wofsy, S. C. (2012). The Amazon basin in transition. *Nature*, *481*(7381), 321–328. https://doi.org/10.1038/nature10717

Ellison, D., Morris, C. E., Locatelli, B., Sheil, D., Cohen, J., Murdiyarso, D., … Sullivan, C. A. (2017). Trees, forests and water: Cool insights for a hot world. *Global Environmental Change*, *43*, 51–61. https://doi.org/10.1016/j.gloenvcha.2017.01.002

ERA5. (2019). *ERA5 reanalysis (0.25 degree latitude-longitude grid)*. https://doi.org/10.5065/BH6N-5N20

Erfanian, A., Wang, G., & Fomenko, L. (2017). Unprecedented drought over tropical South America in 2016: Significantly under-predicted by tropical SST. *Scientific Reports*, *7*(1), 5811. https://doi.org/10.1038/s41598-017-05373-2

Espinoza, J. C., Ronchail, J., Marengo, J. A., & Segura, H. (2019). Contrasting North-South changes in Amazon wet-day and dry-day frequency and related atmospheric features (1981–2017). *Climate Dynamics*, *52*(9), 5413–5430. https://doi.org/10.1007/s00382-018-4462-2

Fan, Y., & van den Dool, H. (2008). A global monthly land surface air temperature analysis for 1948–present. *Journal of Geophysical Research: Atmospheres*, *113*(D1). https://doi.org/10.1029/2007JD008470

Fu, R., Yin, L., Li, W., Arias, P. A., Dickinson, R. E., Huang, L., … Myneni, R. B. (2013). Increased dry-season length over southern Amazonia in recent decades and its implication for future climate projection. *Proceedings of the National Academy of Sciences of the United States of America*, *110*(45), 18110–18115. https://doi.org/10.1073/pnas.1302584110

Gentry, A. H., & Lopez-Parodi, J. (1980). Deforestation and increased flooding of the upper Amazon. *Science*, *210*(4476), 1354–1356. https://doi.org/10.1126/science.210.4476.1354

Gimeno, L., Dominguez, F., Nieto, R., Trigo, R., Drumond, A., Reason, C. J. C., … Marengo, J. (2016). Major mechanisms of atmospheric moisture transport and their role in extreme precipitation events. *Annual Review of Environment and Resources*, *41*(1), 117–141. https://doi.org/10.1146/annurev-environ-110615-085558

Gloor, M., Brienen, R. J. W., Galbraith, D., Feldpausch, T. R., Schöngart, J., Guyot, J.-L., … Phillips, O. L. (2013). Intensification of the Amazon hydrological cycle over the last two decades. *Geophysical Research Letters*, *40*(9), 1729–1733. https://doi.org/10.1002/grl.50377

Hansen, M. C., Potapov, P. V., Moore, R., Hancher, M., Turubanova, S. A., Tyukavina, A., … Townshend, J. R. G. (2013). High-resolution global maps of 21st-century forest cover change. *Science*, *342*(6160), 850–853. https://doi.org/10.1126/science.1244693

Hirota, M., Holmgren, M., Van Nes, E. H., & Scheffer, M. (2011). Global resilience of tropical forest and savanna to critical transitions. *Science*, *334*(6053), 232–235. https://doi.org/10.1126/science.1210657

Hutyra, L. R., Munger, J. W., Nobre, C. A., Saleska, S. R., Vieira, S. A., & Wofsy, S. C. (2005). Climatic variability and vegetation vulnerability in Amazônia. *Geophysical Research Letters*, *32*(24). https://doi.org/10.1029/2005GL024981

Jiménez-Muñoz, J. C., Mattar, C., Barichivich, J., Santamaría-Artigas, A., Takahashi, K., Malhi, Y., … Schrier, G. V. D. (2016). Record-breaking warming and extreme drought in the Amazon rainforest during the course of El Niño 2015–2016. *Scientific Reports*, *6*, 2015–2016. https://doi.org/10.1038/srep33130

Laurance, W. F., Camargo, J. L. C., Fearnside, P. M., Lovejoy, T. E., Williamson, G. B., Mesquita, R. C. G., … Laurance, S. G. W. (2018). An Amazonian rainforest and its fragments as a laboratory of global change. *Biological Reviews*, *93*(1), 223–247. https://doi.org/10.1111/brv.12343

Laurance, W. F., & Williamson, G. B. (2001). Positive feedbacks among forest fragmentation, drought, and climate change in the Amazon. *Conservation Biology*, *15*(6), 1529–1535. https://doi.org/10.1046/j.1523-1739.2001.01093.x

Lawrence, D., & Vandecar, K. (2015). Effects of tropical deforestation on climate and agriculture. *Nature Climate Change*, *5*(1), 27–36. https://doi.org/10.1038/nclimate2430

Li, Y., Zhao, M., Motesharrei, S., Mu, Q., Kalnay, E., & Li, S. (2015). Local cooling and warming effects of forests based on satellite observations. *Nature Communications*, *6*, 1–8. https://doi.org/10.1038/ncomms7603

Lloyd, J., Goulden, M. L., Ometto, J. P., Patiño, S., Fyllas, N. M., & Quesada, C. A. (2009). Ecophysiology of forest and savanna vegetation. *Amazonia and global change* (pp. 463–484). https://doi.org/10.1029/2008GM000741

Malhi, Y., Aragao, L. E. O. C., Galbraith, D., Huntingford, C., Fisher, R., Zelazowski, P., … Meir, P. (2009). Exploring the likelihood and mechanism of a climate-change-induced dieback of the Amazon rainforest. *Proceedings of the National Academy of Sciences of the United States of America*, *106*(49), 20610–20615. https://doi.org/10.1073/pnas.0804619106

Malhi, Y., Roberts, J. T., Betts, R. A., Killeen, T. J., Li, W., & Nobre, C. A. (2008). Climate change, deforestation, and the fate of the Amazon. *Science*, *319*(5860), 169–172. https://doi.org/10.1126/science.1146961

Messina, J. P., & Cochrane, M. A. (2007). The forests are bleeding: How land use change is creating a new fire regime in the Ecuadorian Amazon. *Journal of Latin American Geography*, *6*(1), 85–100. https://doi.org/10.1353/lag.2007.0007

Negrón-Juárez, R. I., Holm, J. A., Marra, D. M., Rifai, S. W., Riley, W. J., Chambers, J. Q., … Higuchi, N. (2018). Vulnerability of Amazon forests to storm-driven tree mortality. *Environmental Research Letters*, *13*(5), 54021. https://doi.org/10.1088/1748-9326/aabe9f

Nepstad, D., Lefebvre, P., Lopes da Silva, U., Tomasella, J., Schlesinger, P., Solorzano, L., … Guerreira Benito, J. (2004). Amazon drought and its implications for forest flammability and tree growth: A basin-wide analysis. *Global Change Biology*, *10*(5), 704–717. https://doi.org/10.1111/j.1529-8817.2003.00772.x

Nepstad, D. C., Tohver, I. M., David, R., Moutinho, P., & Cardinot, G. (2007). Mortality of large trees and lianas following experimental drought in an Amazon forest. *Ecology*, *88*(9), 2259–2269. https://doi.org/10.1890/06-1046.1

Nobre, C. A., Sampaio, G., Borma, L. S., Castilla-Rubio, J. C., Silva, J. S., & Cardoso, M. (2016). Land-use and climate change risks in the amazon and the need of a novel sustainable development paradigm. *Proceedings of the National Academy of Sciences of the United States of America*, *113*(39), 10759–10768. https://doi.org/10.1073/pnas.1605516113

Otón, G., Ramo, R., Lizundia-Loiola, J., & Chuvieco, E. (2019). Global detection of long-term (1982–2017) burned area with AVHRR-LTDR data. *Remote Sensing*, *11*, 1982–2017. https://doi.org/10.3390/rs11182079

Palmer, W. C. (1965). *Meteorological drought*. Technique Report Weather Bureau Research Paper No. 45. Washington, DC: Office

of Climatology, U.S. Weather Bureau. Retrieved from https://www.ncdc.noaa.gov/temp-and-precip/drought/docs/palmer.pdf

Phillips, O. L., van der Heijden, G., Lewis, S. L., López-González, G., Aragão, L. E. O. C., Lloyd, J., … Vilanova, E. (2010). Drought–mortality relationships for tropical forests. *New Phytologist*, *187*(3), 631–646. https://doi.org/10.1111/j.1469-8137.2010.03359.x

Qin, Y., Xiao, X., Dong, J., Zhang, Y., Wu, X., Shimabukuro, Y., … Moore, B. (2019). Improved estimates of forest cover and loss in the Brazilian Amazon in 2000–2017. *Nature Sustainability*, *2*(8), 764–772. https://doi.org/10.1038/s41893-019-0336-9

Randerson, J. T., van der Werf, G. R., Giglio, L., Collatz, G. J., & Kasibhatla, P. S. (2018). *Global fire emissions database, version 4.1 (GFEDv4)*. Oak Ridge, TN: ORNL DAAC. Retrieved from https://doi.org/10.3334/ORNLDAAC/1293

Running, S., Mu, Q., & Zhao, M. (2017). *MOD16A2 MODIS/Terra Net Evapotranspiration 8-Day L4 Global 500m SIN Grid V006*. https://doi.org/10.5067/MODIS/MOD16A2.006

Saatchi, S., Asefi-Najafabady, S., Malhi, Y., Aragão, L. E. O. C., Anderson, L. O., Myneni, R. B., & Nemani, R. (2013). Persistent effects of a severe drought on Amazonian forest canopy. *Proceedings of the National Academy of Sciences of the United States of America*, *110*(2), 565–570. https://doi.org/10.1073/pnas.1204651110

Schaaf, C., & Wang, Z. (2015). *MCD43C3 MODIS/Terra+Aqua BRDF/Albedo Albedo Daily L3 Global 0.05Deg CMG V006*. https://doi.org/10.5067/MODIS/MCD43C3.006

Schneider, U., Becker, A., Finger, P., Meyer-Christoffer, A., Rudolf, B., & Ziese, M. (2011). *GPCC full data reanalysis version 6.0 at 0.5°: Monthly land-surface precipitation from rain-gauges built on GTS-based and historic data*. https://doi.org/10.5676/DWD_GPCC/FD_M_V7_050

Skansi, M. D. L. M., Brunet, M., Sigró, J., Aguilar, E., Arevalo Groening, J. A., Bentancur, O. J., … Jones, P. D. (2013). Warming and wetting signals emerging from analysis of changes in climate extreme indices over South America. *Global and Planetary Change*, *100*, 295–307. https://doi.org/10.1016/j.gloplacha.2012.11.004

Staal, A., Flores, B. M., Aguiar, A. P. D., Bosmans, J. H. C., Fetzer, I., & Tuinenburg, O. A. (2020). Feedback between drought and deforestation in the Amazon. *Environmental Research Letters*, *15*(4), 44024. https://doi.org/10.1088/1748-9326/ab738e

Staal, A., Tuinenburg, O. A., Bosmans, J. H. C., Holmgren, M., van Nes, E. H., Scheffer, M., … Dekker, S. C. (2018). Forest-rainfall cascades buffer against drought across the Amazon. *Nature Climate Change*, *8*(6), 539–543. https://doi.org/10.1038/s41558-018-0177-y

Stephens, S. L., Collins, B. M., Fettig, C. J., Finney, M. A., Hoffman, C. M., Knapp, E. E., … Wayman, R. B. (2018). Drought, tree mortality, and wildfire in forests adapted to frequent fire. *BioScience*, *68*(2), 77–88. https://doi.org/10.1093/biosci/bix146

Taufik, M., Torfs, P. J. J. F., Uijlenhoet, R., Jones, P. D., Murdiyarso, D., & Van Lanen, H. A. J. (2017). Amplification of wildfire area burnt by hydrological drought in the humid tropics. *Nature Climate Change*, *7*, 428–431. https://doi.org/10.1038/nclimate3280

Trenberth, K. E., Dai, A., Van Der Schrier, G., Jones, P. D., Barichivich, J., Briffa, K. R., & Sheffield, J. (2014). Global warming and changes in drought. *Nature Climate Change*, *4*(1), 17–22. https://doi.org/10.1038/nclimate2067

Uhl, C. (1998). Perspectives on wildfire in the humid tropics. *Conservation Biology*, *12*(5), 942–943. https://doi.org/10.1046/j.1523-1739.1998.012005942.x

Uhl, C., & Kauffman, J. B. (1990). Deforestation, fire susceptibility, and potential tree responses to fire in the eastern Amazon. *Ecology*, *71*(2), 437–449. https://doi.org/10.2307/1940299

van der Schrier, G., Barichivich, J., Briffa, K. R., & Jones, P. D. (2013). A scPDSI-based global data set of dry and wet spells for 1901–2009. *Journal of Geophysical Research: Atmospheres*, *118*(10), 4025–4048. https://doi.org/10.1002/jgrd.50355

Wan, Z., Hook, S., & Hulley, G. (2015). *MYD11C2 MODIS/aqua land surface temperature/emissivity 8-day L3 global 0.05Deg CMG V006. 2015*. https://doi.org/10.5067/MODIS/MYD11C2.006

Wright, J. S., Fu, R., Worden, J. R., Chakraborty, S., Clinton, N. E., Risi, C., … Yin, L. (2017). Rainforest-initiated wet season onset over the southern Amazon. *Proceedings of the National Academy of Sciences of the United States of America*, *114*(32), 8481–8486. https://doi.org/10.1073/pnas.1621516114

Yoon, J.-H., & Zeng, N. (2010). An Atlantic influence on Amazon rainfall. *Climate Dynamics*, *34*(2), 249–264. https://doi.org/10.1007/s00382-009-0551-6

Zemp, D. C., Schleussner, C.-F., Barbosa, H. M. J., Hirota, M., Montade, V., Sampaio, G., … Rammig, A. (2017). Self-amplified Amazon forest loss due to vegetation-atmosphere feedbacks. *Nature Communications*, *8*, 1–10. https://doi.org/10.1038/ncomms14681

Zeng, N., Yoon, J.-H., Marengo, J. A., Subramaniam, A., Nobre, C. A., Mariotti, A., & Neelin, J. D. (2008). Causes and impacts of the 2005 Amazon drought. *Environmental Research Letters*, *3*(1), 14002. https://doi.org/10.1088/1748-9326/3/1/014002

Zhang, M., Liu, N., Harper, R., Li, Q., Liu, K., Wei, X., … Liu, S. (2017). A global review on hydrological responses to forest change across multiple spatial scales: Importance of scale, climate, forest type and hydrological regime. *Journal of Hydrology*, *546*, 44–59. https://doi.org/10.1016/j.jhydrol.2016.12.040

SUPPORTING INFORMATION

Additional supporting information may be found online in the Supporting Information section.

How to cite this article: Xu X, Jia G, Zhang X, Riley WJ, Xue Y. Climate regime shift and forest loss amplify fire in Amazonian forests. *Glob Change Biol*. 2020;26:5874–5885. https://doi.org/10.1111/gcb.15279